

Neural message passing for predicting abnormal grain growth in Monte Carlo simulations of microstructural evolution

Ryan Cohn, Elizabeth A. Holm

Department of Materials Science. Carnegie Mellon University. Pittsburgh, PA, USA

October 18, 2021

Abstract

Abnormal grain growth can significantly alter the properties of materials during processing. This can cause significant variation in the properties and performance of in-spec feedstock components subjected to identical processing paths. Understanding and controlling abnormal grain growth has proved to be elusive due to the stochastic nature of this phenomenon. However, recent advances in deep learning provide a promising alternative to traditional experimental and physics-based methods for understanding this phenomenon. Neural message passing allows deep learning to be applied to irregular inputs including graph representations of grain structures in a material. In this study we generate a large database of Monte Carlo simulations of abnormal grain growth in an idealized system. We apply message passing neural networks to predict the occurrence of abnormal grain growth in these simulations using only the initial state of the system as input. A computer vision model is also trained for the same task for comparison. The preliminary results indicate that the message passing approach outperforms the computer vision method and achieved 75% prediction accuracy, significantly better than random guessing. Analysis of the uncertainty in the Monte Carlo simulations provides a road map for ongoing work on this project.

1 Introduction

1.1 Abnormal grain growth

Abnormal grain growth (AGG) occurs when the growth rate of a small subset of grains significantly exceeds that of their neighbors. The resulting change in grain size distribution may significantly alter the properties of the material. A clear example of a grain that has undergone AGG, growing significantly larger than all of its neighboring grains in the matrix, is shown in Figure 1. AGG is often desirable in materials such as silicon transformer steels [1] and materials for interior permanent magnets [2] as larger grains lead to enhanced magnetic properties. However, AGG can be detrimental to structural materials where the presence of larger grains in the matrix can reduce the fatigue strength of materials [3]. One anonymous industrial supplier notes that AGG can cause about 1/3 of parts to fail after processing, despite originally being in-spec with seemingly identical properties. This is associated with an estimated cost of \$10 million/year for the supplier.

Regardless of whether AGG is to be encouraged or prevented it is desirable to understand and control AGG during processing to optimize the properties of various materials. Thus, researchers are actively investigating AGG with the goal of understanding and controlling this phenomenon [4–8].

Despite the advances made in this area, including understanding of AGG in a statistical manner, researchers have not been able to predict which individual samples will undergo AGG during processing. Additionally, researchers have not been able to observe regions of the initial microstructure where AGG occurs in samples. There are multiple reasons why observing and predicting AGG are so difficult. First, AGG is considered to be a rare event. The fraction of grains that may undergo AGG is system dependent, but in a typical material it may occur on the order of 1 in 20,000 to 1 in 100,000 grains. Thus, it is not feasible to image large enough regions to capture AGG in-situ. After processing, AGG is obvious, as some grains may grow so large they may be visible to the naked eye. However, the process of AGG results in the consumption of the original neighborhood of the abnormal grain. Thus, most of the information contained

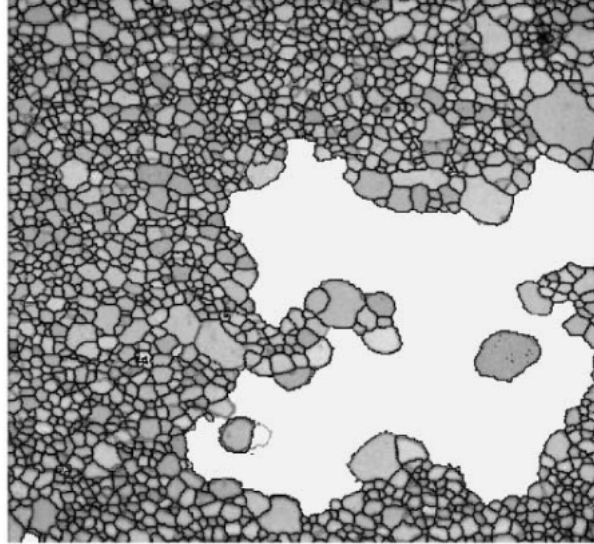


Figure 1: Orientation Image Microscopy image of abnormal Goss grain (white) in Fe-3%Si steels. Image source: Figure 4b in ref [1]

in the initial state of the system is lost, preventing researchers from determining the factors that enabled a specific grain to grow abnormally.

Therefore, without already having a predictive model to indicate where AGG will occur, it is unclear where to look. However, generating a model to identify regions where AGG is likely to occur requires existing data for training. This creates a paradox, as the model is needed to generate data, but data is needed to train the model. Thus, to avoid the limitations of experiments, we instead turn to simulations.

DeCost applied Monte Carlo analysis to model AGG in an idealized system [9] with nonuniform grain boundary mobility values. The fraction of higher mobility grain boundaries was varied to determine if nonuniform grain boundary mobility can act as a persistence mechanism to sustain AGG in the system. The results supported this idea, at least for the idealized system used in the simulation. Additionally, analysis of simulations that did exhibit AGG indicated a possible mechanism for the process. Rather than a consistently high growth rate, it was observed that AGG occurs through a series of localized rapid growth events in which the abnormal grain consumed the neighboring grains. This indicates that AGG depends on more than just the immediate neighbors of a grain, making it difficult to model. AGG was characterized in a statistical sense, but no attempt was made to create a predictive model to identify which simulations exhibit AGG. In this study we build upon the foundational work set by DeCost. We develop a database of the same types of grain growth simulations with the goal of developing a predictive model to identify which trials will undergo AGG.

1.2 Graphs and message passing neural networks

For modeling the initial grain structure of the system it is desirable to preserve the local connectivity of each grain. Thus, graph-based representations offer an attractive alternative to image or feature based representations that are commonly used as inputs for deep learning models.

A graph is a data structure consisting of vertices, also called nodes, that are connected by edges, also called links. Nodes, edges, and graphs can each have feature descriptors associated with them. Thus, graphs are very flexible and expressive data structures. However, a consequence of this is that graphs may have very irregular structures. For example, two different graphs may have different numbers of nodes and edges, and different nodes in the same graph may have different numbers of neighboring nodes. Thus, conventional neural network architectures, which require a fixed input size, can not be used to analyze datasets containing graphs with different structures.

To overcome this limitation and apply deep learning to graphs with different structures, researchers developed neural message passing [10], which has been applied to a wide range of applications including predicting molecular properties [10], learning physical relations [11], and more [12–14].

In the message passing framework, a graph contains a node feature matrix and an edge matrix. The node feature matrix is a matrix where each row gives the feature vector for the corresponding node in the graph. The edge matrix is a matrix where each row contains the index of the source and target node (consistent with the indexing in the node feature matrix) that are connected by the corresponding edge. Optionally, an edge feature matrix and graph feature vector may be associated with the graph and included during the message passing process, but these are omitted in the description for the sake of simplicity.

During each iteration i of message passing a hidden state, denoted \mathbf{h}^i , is associated with every node u on the graph. The initial hidden state, \mathbf{h}^0 , is the node feature matrix. Then, for each next iteration of message passing, the hidden state is updated according to the following process.

$$\mathbf{h}_u^{i+1} = \text{UPDATE}(\mathbf{h}_u^i, \text{AGGREGATE}(\{\text{MESSAGE}(\mathbf{h}_v^i, \forall v \in N(u))\})) \quad (1)$$

In this equation, $v \in N(u)$ denotes all nodes v than are neighbors (connected by an edge) of node u . MESSAGE and UPDATE can be any differentiable functions, such as neural networks. AGGREGATE can be any differentiable, permutation-invariant set function such as min, max, mean, sum, etc.

In plain English message passing works through the following steps: First, for a given target node the message of each neighboring node is computed by applying a differentiable transformation to the neighboring node’s hidden state. Next, the messages from all nodes in the neighborhood are aggregated into one signal. Finally, the aggregated messages, along with the current hidden state of the target node, are transformed to compute the new hidden state of the target node. Repeating this process for each node in the graph constitutes one iteration of message passing. The message passing process is repeated for the desired number of iterations. The final hidden states of each node can be used as inputs to a separate function to generate node-level outputs (for example, a classification label for each node), or can be aggregated into a single state used to make graph-level predictions (for example, a prediction of a molecular property.)

The message passing algorithm has two especially desirable properties for analyzing graph-based data. The first is the use of the aggregation function. Note that the output of the aggregation function does not directly depend on the number or ordering of incoming messages. This ensures that outputs of message passing are invariant to graph isomorphism and the same model can be used to analyze nodes with different numbers of neighbors. This is essential for analyzing grain structures which have no natural ordering and contain grains with different numbers of neighbors.

The second important feature is after k iterations of message passing, information from a given node u is propagated to nodes that are within k -hops of u . This can be used to determine how much relevant information is included in each neighborhood shell of a given node. This shows promise for better understanding the influence of each neighborhood shell on AGG which is a question of particular interest.

1.3 Hypotheses

There are two main hypotheses of this study.

- Deep learning methods can be used to predict the occurrence of AGG in ‘candidate grain’ SPPARKS simulations using only the initial state of the system as an input with at least 80% prediction accuracy.
- Using graph-based approaches like neural message passing will achieve higher classification accuracy scores than a typical computer vision based approach.

To be objective, quantitative, and falsifiable, both of the above hypotheses need several qualifiers. In the first hypothesis, the 80% classification accuracy refers to the performance on the hidden test set of the dataset used in this study, which is introduced in Section 2.1. The threshold of 80% was selected as a best guess of the expected performance of the approach. It is established that deep learning approaches can achieve very high performance of over 95% on reasonably complex tasks such as image classification. However, AGG is a more difficult problem and unlike image classification humans cannot predict which microstructures will undergo AGG with high probability. Additionally, the stochastic nature of Monte Carlo simulations limits

the maximum possible accuracy that can be achieved. This is investigated and discussed in further detail in Section 4. Thus, deep learning models are not expected to achieve the same level of predictive performance on this task.

For the second hypothesis it is important to note that there is no established standard computer vision approach for the task of predicting microstructural evolution from image-based representations of a grain structure. Thus, graph based approach outperforming a computer vision approach does not prove that certain graph based approaches will perform better than any possible computer vision pipeline, and the reverse is also true. In an attempt to provide a reasonable comparison between the two approaches, the computer vision approach used in this study was validated on a separate dataset. This confirmed that the approach was sufficiently sophisticated to capture relevant features in images yet simple enough to be trained on a relatively small dataset similar in size to the one used in this study. Though it cannot be proved definitively, it is expected that the graph-based approach will achieve higher performance due to the ability of graphs to preserve the exact connectivity of grains in the original microstructure, which is not possible with images.

2 Methods

2.1 Dataset creation

SPPARKS [15, 16] was used to generate a dataset of ‘candidate grain’ growth simulations using the same approach as DeCost. The simulations are summarized here but more detailed information is available in ref [9].

The system contains a rectangular grid of pixels with integer identifiers. Grains in the matrix consist of groups of connected pixels with the same identity. One grain, termed the ‘candidate grain’, has an initial size advantage compared to the rest of the matrix grains. The rest of the matrix consists of ‘red’ and ‘blue’ grains. The grain boundary energy for all interfaces is uniform. The red/candidate interfaces are artificially assigned a high value for grain boundary mobility, and all other interfaces are assigned a lower mobility. During the Monte Carlo simulation a site in the matrix is selected randomly. The probability of changing states from one grain to another, which is related to both the mobility of the interface and the energy associated with changing states, is computed. The change is randomly accepted or rejected with the probability computed in the previous step. This process is repeated for a very large number of iterations. During this process the flipping of states causes some grains to grow and other grains to shrink, modeling grain growth in real materials. After repeating this process for the desired number of iterations the final state of the system is recorded.

In this study all simulations were run with a system size of 512 x 512 pixels using periodic boundary conditions, a Monte Carlo temperature of $kT=0.9$, and a duration of 4,000,000 Monte Carlo steps. The fraction of red grains was varied between 0 and 0.4. However, 90% of the simulations contained fractions of red grains between 0.15 and 0.25, the region where the occurrence of AGG is most uncertain (about half of these trials exhibit AGG.) Example grain growth trajectories from two simulations are shown in Figure 2. The top and bottom rows show snapshots from sample trajectories for normal and abnormal grain growth, respectively.

27,588 simulations were run. The data were divided into two datasets, one larger and one smaller. The first dataset, termed the ‘full dataset’, contains all of the simulations. This dataset was randomly divided into a training set containing 25,588 trials, a validation set containing 1000 trials, and a test set containing 1000 trials. The second dataset, termed the ‘small dataset’ contains a much smaller number of simulations. This set contains 1000 training, 100 validation, and 100 test simulations. Each subset was randomly sampled from the corresponding subset in the full dataset to maintain consistency of the validation and test sets.

Note that the exact definition of AGG is subjective. However, training a predictive classification model requires an objective definition of the output. Thus, the first step in this study was to determine a working definition of AGG. In ref [9], growth of the candidate grain is determined to be abnormal when the final area of the candidate grain is at least 6 times the area of an average grain in the matrix. However, due to its initial size advantage, the candidate grain almost always outgrows typical matrix grains by a significant amount, prompting an investigation into the significance of this definition.

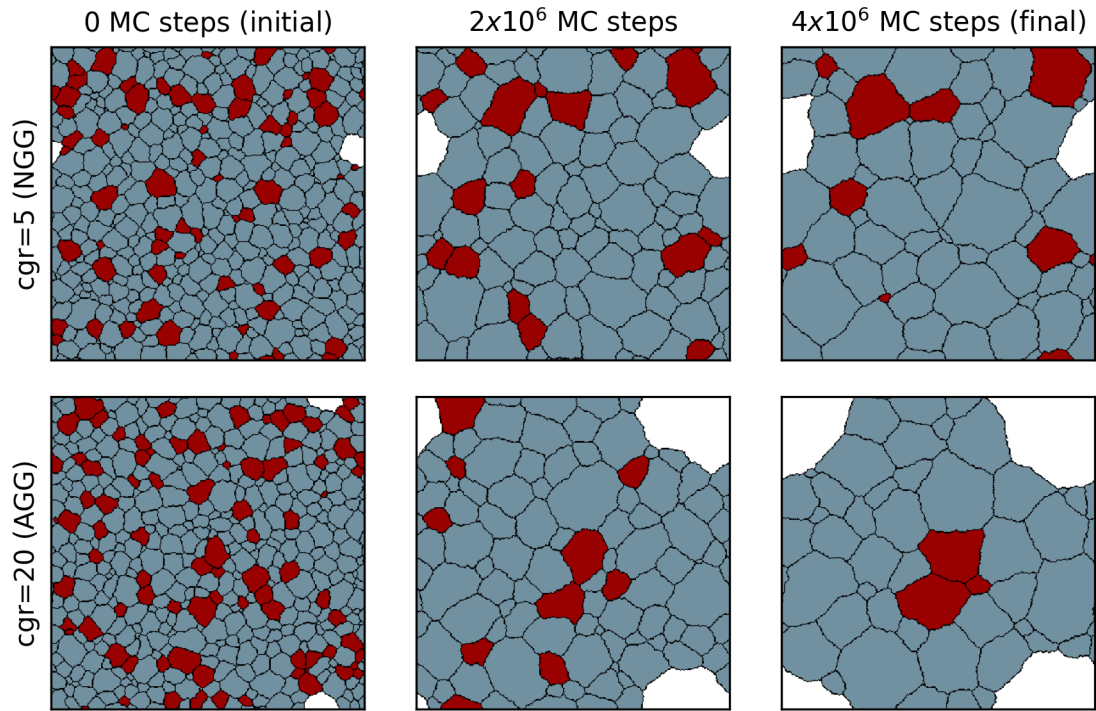


Figure 2: Sample grain evolution for candidate growth ratio values of 5 (top), representing normal growth, and 20 (bottom), representing abnormal growth. Snapshots of the microsture are shown after of 0 (left), 2,000,000 (middle), and 4,000,000 (right) Monte Carlo time steps. The candidate grain is shown in white. Note that the candidate grain ‘wraps around’ the edges of the images due to the use of periodic boundary conditions in the simulations.

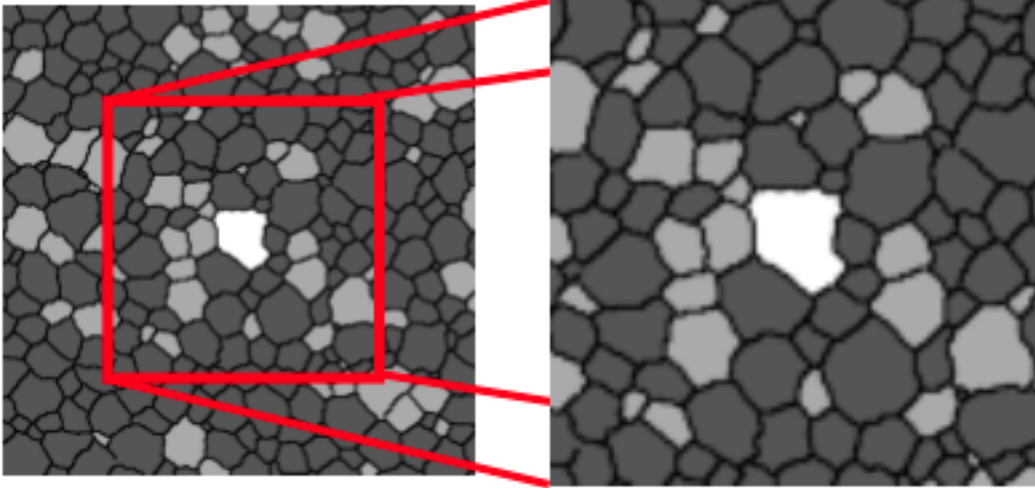


Figure 3: Left: Grayscale image representation of the initial microstructure. Right: Cropped image representation which includes a smaller neighborhood of the system.)

In this study, AGG is characterized by the "candidate growth ratio," or CGR, which is the ratio of the final size of the candidate grain to its initial size. After manual analysis of several of the simulations, a preliminary definition of AGG was determined as follows: AGG occurs when the candidate growth ratio is at least 10. The justification for this criteria is that all of the manually observed trials where the candidate grain increased in size by a factor of 10 clearly exhibited AGG. Grain growth occurred with sudden bursts of growth through high mobility interfaces, and the candidate grain ended up significantly larger than neighboring grains compared to trials that did not exhibit AGG. After selecting this criteria, the labels were compared to the criteria used in ref [9]. Despite having different simulation parameters, 90% of the labels (normal vs abnormal) agreed with each other. This validates both criteria as being reasonably consistent ways to classify AGG. In this study, the growth ratio threshold of 10 is used for determining AGG.

This criteria was selected to only include significant observations of AGG. This minimizes the number of false positive labels for AGG. This is beneficial for the eventual goal of helping experimentalists find regions that are likely to undergo AGG. In this case missing some regions where AGG is likely to occur is less costly than falsely predicting AGG will occur when in reality it does not. Note that for use with a quality control setting, it may be better to use a different criteria for AGG that achieves a desirable balance between false positives and false negatives.

2.2 Baseline model: computer vision and transfer learning

A computer vision approach for predicting the occurrence of AGG from the initial state of the system was evaluated as a baseline approach for comparison. The output of the SPPARKS simulations include an image with pixel values equal to the integer identifier of the grain that the pixel belongs to. The preprocessing steps for using these images with the computer vision approach are as follows.

First, the grains are assigned grayscale intensity values corresponding to their identity. Pixels in blue, red, and the candidate grains are assigned values of $1/3$, $2/3$, and 1 , respectively. Next, pixels on the boundaries of each grain were assigned intensity values of 0 . This allows adjacent grains with the same ID to be distinguished from each other. Finally, the coordinates of the image were shifted such that the candidate grain is always centered in the image. This can be done because the simulations were run with periodic boundary conditions. Two sets of images were produced. In the first, the representation of the entire microstructure was resized into a 224×224 image to ensure the size was compatible with a pre-trained neural network. In the second, images were evenly cropped down to a size of 224×224 , which typically included up to 4th nearest neighbors of the candidate grain. Sample full and cropped images after pre-processing are shown in Figure 3.

After pre-processing the images, a pre-trained convolutional neural network was used as a feature extractor in a transfer learning approach. VGG16 [17], pre-trained on ImageNet [18], was used to process the images. The outputs of the first fully connected (fc1) layer were used as feature descriptors for each image. Principal component analysis (PCA) [19] was applied to reduce the dimensions of the fc1 feature vectors from 4096 to 50 dimensions. Using 50 dimensions preserved 77% of the variance in both training sets of images. Finally, a support vector machine (SVM) [20] with a radial basis function kernel was trained to predict whether or not a candidate growth ratio greater than 10 would be achieved from a given initial state. The validation set was used to tune the regularization hyperparameter C . This parameter determines the trade-off between a larger margin (low values of C) and fewer misclassified points in the training set (high values of C .) During training C was varied between values of 10^{-2} and 10^2 . The model with the lowest validation error during training was used.

Note that this method is only a single approach to predicting AGG from an image based representation of the initial state of the system. To justify the use of this approach as a representative baseline for computer vision, this method was benchmarked on a standard image classification task in materials science. The Northeastern University Steel Surface Defects dataset [21] is an established dataset containing images of defects on hot rolled steel that can be used to quickly evaluate image classification models. This is covered in more detail in ref [22]. The images were pre-processed by applying contrast-limited adaptive histogram equalization to remove the effects of relative brightness and then resizing so the images could be passed through VGG16. The rest of the analysis was identical to the above mentioned process, consisting of extracting features from the fc1 layer of VGG16, applying PCA to reduce the dimensionality to 50 (preserving 74% of the variance,) and classifying the images with an SVM with a radial basis function kernel. For this task, a default value of 1 for the regularization parameter C was used. Five fold cross validation was used to evaluate the model and the performance is shown in Table 1. Even without hyperparameter tuning, the approach achieves higher than 99% accuracy in each of the cross validation folds, including two trials with perfect classification of the validation set. This suggests that the transfer learning approach used in this study is capable of capturing relevant features in real images of materials.

Fold	1	2	3	4	5
Validation accuracy	0.997	0.994	1.000	1.000	0.997

Table 1: Cross-validation accuracy of the computer vision approach on the Northeastern University Steel Surface Defects Dataset.

2.3 Graph-based model: simple graph convolution network

Before applying a graph neural network to predict the occurrence of AGG, the output from SPPARKS must first be represented as a graph. This process involves two steps. First, the connectivity of grains to their nearest neighbors must be determined. Next, the features for the nodes are extracted. Note that edge and graph level features may also be extracted. However, most off-the-shelf models only utilize node features. Thus, in this study, only node features are used to describe the properties of the graph. Using more sophisticated models that incorporate edge and graph level features may lead to better performance and is one possible direction for future research efforts.

The process for determining the neighborhood connectivity of each grain is as follows. First, the coordinates of the system are rolled to center the grain. This eliminates variations due to grains located on or wrapped around the edges of the system. Next, binary dilation with a 3x3 square structuring element is applied to the grain. The set of other grains that overlap the dilated grain of interest are determined to be in its neighborhood. This process was repeated for all grains in the system.

In this study, the features associated with each node (grain) were as follows. The ‘type’ of grain (red/blue/candidate) was read directly from the SPPARKS outputs. The node degree, or number of nearest neighbors associated with a grain, was determined from the connectivity of the graph. Finally, the area, perimeter, equivalent circle diameter, major axis length, and minor axis length of the grain were measured from the pixels included in each grain. These measurements were generated from scikit-image [23] with the `skimage.measure.regionprops_table` function.

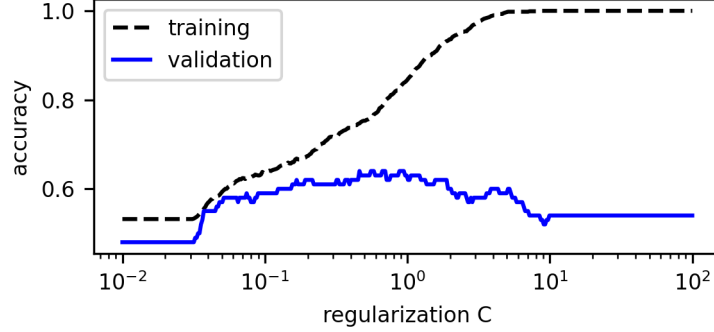


Figure 4: Training and validation accuracy for SVM trained on features extracted from full images plotted against regularization parameter C .

After extracting a graph-based representation, a Simple Graph Convolution (SGC) [24] model was trained on the data. SGC involves message passing with K -step feature propagation. During each iteration of message passing, the hidden states of all nodes in the neighborhood of a target node (including the state of the target node) are averaged together to determine the new state of the target node. This process is repeated for K iterations. Afterwards, node classification is achieved by passing the final hidden state of a given node through a linear logistic regression classifier. Interestingly, this approach is linear and does not contain any trainable parameters until the final logistic regression classifier. Thus, it is a much simpler model than other graph convolution approaches. Despite this, SGC achieves accuracy scores comparable to much more complex methods on standard benchmark graph datasets like Cora [25] and CiteSeer [12].

SGC models were trained on the training set for 200 epochs. The performance on the training and validation sets were measured at the end of every 10 training epochs and the model with the lowest validation loss was used for the final evaluation. During training the negative log likelihood loss function was used to measure the distance between the predicted and true values for training examples. The Adam optimizer [26] was used to update the model parameters during backpropagation.

A couple different learning rates and weight decay parameters were tried. The results are reported for a learning rate of 0.005 and a weight decay of 0.001 as they gave reasonable results for model training. Future plans for scaling up the model include a more thorough grid search to tune these parameters. K , the number of neighborhood hops to include during the message passing process, was varied between 1 and 4 to determine how the number of neighborhood shells influences the performance. Each model was trained for 200 epochs. During training the average training and validation losses were recorded every 10 epochs. The model with the lowest validation loss was evaluated on the train, validation, and test sets.

3 Results and discussion

3.1 Predictive model- computer vision

The first SVM model was trained on features extracted from images of the entire initial microstructure. The training and validation accuracy scores for different values of the regularization parameter C are shown in Figure 4. As C is increased to values above 8.5, the model achieves perfect classification of the training set. However, this performance does not generalize and the performance on the validation set is only around 54%, indicating the occurrence of overfitting. Using $C=0.46$ gives a maximum validation accuracy of 0.64. This value was used for the final evaluation of the model on the test set. The confusion matrices for the final model on the training, validation, and test sets are shown in Figure 5. The model achieves training, validation, and test accuracy scores of 0.75, 0.64, and 0.60, respectively. The biggest source of classification errors in all 3 of the datasets is falsely predicting that the candidate grain would grow abnormally when it instead undergoes normal grain growth during the simulation. This leads to very low recall scores for predictions of normal grain growth in the validation and test sets with values 0.42 and 0.35, respectively. The training set is slightly unbalanced, with 53% of the initial states demonstrating AGG. To verify that the

	Training		Validation		Test	
True value	NGG	AGG	NGG	AGG	NGG	AGG
	278	190	22	30	18	33
Predicted Value	NGG	AGG	NGG	AGG	NGG	AGG
	63	469	6	42	7	42

Figure 5: Confusion matrices for SVM trained on features from full images on training (left), validation (middle), and test (right) sets. "NGG" and "AGG" denote normal and abnormal grain growth, respectively.

model was not biased towards predicting that most runs will exhibit AGG due to the uneven distribution of training examples, another SVM was trained with the same parameters. During training, the loss component of each example was weighted inversely to the frequency of the labels in the dataset, reducing the effect of class imbalance. This did not significantly change the resulting model performance, confirming that the low classification performance is not simply a result of the presence of the imbalanced dataset.

The images contained the entire initial microstructure. However, it is unlikely that grains far away from the candidate have significant influence over its growth trajectory. Thus, a second set of tests was conducted using cropped images. 224x224 patches were extracted from the center of each image. This captured about 4 neighborhood shells of the candidate grain and also removed artifacts from image preprocessing as these patches did not need to be resized before feature extraction. The training and validation accuracy scores for different values of the regularization parameter C are shown in Figure 6. Setting $C=0.067$ achieves a maximum validation accuracy of 0.74. Interestingly, the validation accuracy is actually higher than the training accuracy. This may be an artifact of the small dataset size.

The confusion matrices for predictions on the training, validation, and test set are shown in Figure 7. The classification accuracy scores on the training, validation, and test sets are 0.67, 0.74, and 0.62, respectively. Since neither model achieved higher than 80% classification accuracy on the datasets, the first hypothesis remains unsupported. However, the results still provide a useful baseline for the performance of the graph-based model to be compared against.

Despite having better performance on the validation set, the model performance does not generalize well and shows a similar classification test accuracy to the model trained on full images. Similar to before, the largest source of error was falsely predicting AGG in trials that underwent normal grain growth. One possible explanation of the low performance is that the training set did not contain enough data to train the model. However, the computer vision approach was validated on the NEU dataset before being used in this experiment. During cross-validation, only about 240 images from each defect class were used for model training, and the model still achieved over 99% validation accuracy in each fold. Though the classification performance on the NEU dataset is not guaranteed to be transferable to other datasets, it does demonstrate how the proposed computer vision approach can be used to successfully classify different images with a small number of training images.

In this study, the training set in this study includes 468 and 532 images of microstructures that exhibited normal and AGG, respectively. Thus, this indicates that predicting the occurrence of AGG (as defined in this study) from an image representation of the initial microstructure is a more difficult challenge, and the lower performance is not simply a result of having not enough training images to successfully fit the model. Nonetheless, the plans for future research include repeating this experiment using a larger dataset with over 27,000 images to train and test the model. This will determine if simply adding more training examples will lead to improved classification performance.

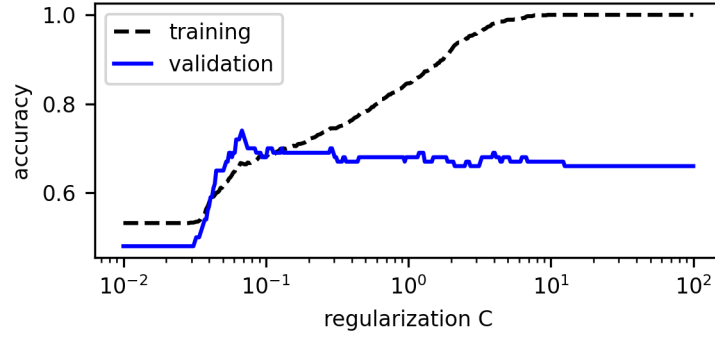


Figure 6: Training and validation accuracy for SVM trained on features extracted from cropped images as a function of regularization parameter C .

		Training		Validation		Test	
True value	NGG	191	277	30	22	20	31
	AGG	57	475	4	44	7	42
		NGG		AGG		NGG	
		Predicted Value		Predicted Value		Predicted Value	

Figure 7: Confusion matrices for SVM trained on features from cropped images on training (left), validation (middle), and test (right) sets. "NGG" and "AGG" denote normal and abnormal grain growth, respectively.

		Training		Validation		Test	
True value	NGG	270	198	36	16	32	19
	AGG	93	439	9	39	6	43
		NGG	AGG	NGG	AGG	NGG	AGG
		Predicted Value		Predicted Value		Predicted Value	

Figure 8: Confusion matrices for SGC model with K=2 on training (left), validation (middle), and test (right) sets. "NGG" and "AGG" denote normal and abnormal grain growth, respectively.

3.2 Predictive model- simple graph convolution

The confusion matrices for the Simple Graph Convolution model with K=2 is shown in Figure 8. The model achieves classification accuracy scores of 0.71, 0.75, and 0.75 on the training, validation, and test sets, respectively. Compared to the computer vision approach the simple graph convolution model demonstrates much better classification performance. Not only are the classification scores higher, but the performance on the training, validation, and test sets are much closer to each other. This indicates that the SGC model does not over-fit the data and generalizes to unseen examples much better than the computer vision approach.

Similar to the computer vision approach, the biggest source of classification error is falsely predicting AGG in trials that undergo normal grain growth. It is possible that weighting the loss components during training or even balancing the dataset would help even out the ratio of false positive and false negative predictions of AGG. However, since there is only slight imbalance in the dataset, and the model still makes a significant number of predictions of normal grain growth, the unbalanced dataset is unlikely to be the sole source of errors in predictions. This is consistent with the results in Section 3.1 where weighting the loss components did not change the performance of the model by a significant amount.

Separate models were trained with K varying from 1 to 4. This allows for direct measurement of how the number of neighborhood shells included in the analysis effects the predictive performance of each model. The training, validation, and test accuracy for these models trained are shown in Figure 9. With K=1, the model achieves very low classification accuracy around 0.55 on the validation and test sets. As K is increased to 2, the classification performance increases to 0.75. As K is increased to values of 3 and 4, the classification accuracy does not change much and remains around 0.73. These results suggest that all of the relevant information for maximizing the predictive performance of AGG is contained in the nearest and next-nearest neighbors of the candidate grain. This result highlights a key advantage of the message passing approach. By preserving the connectivity of the grain structure in the graph data structure, it is possible to examine the effect of including different subsets of grains on the performance of the model. This type of analysis is not possible with computer vision approaches which require rectangular input images.

The maximum accuracy score achieved by the SGC model was around 75%. Thus, the first hypothesis, stating that the data can be classified with over 80% accuracy, remains unsupported. However, the performance of the SGC model surpassed that of the computer vision approach. In addition to achieving higher accuracy scores, the SGC model demonstrated the ability to generalize to the test set much better. This supports the second hypothesis proposed in this study that preserving graph structure is important to detecting AGG in the material.

4 Estimation of the maximum meaningful prediction accuracy

As detailed above, the SGC model significantly outperforms the computer vision approach for predicting the occurrence of AGG from the initial microstructure in this dataset. However, the performance of the SGC model is far from perfect with a 25% error rate. There are several possible changes that can be made to the process to improve the classification performance including using a different set of node features, a more

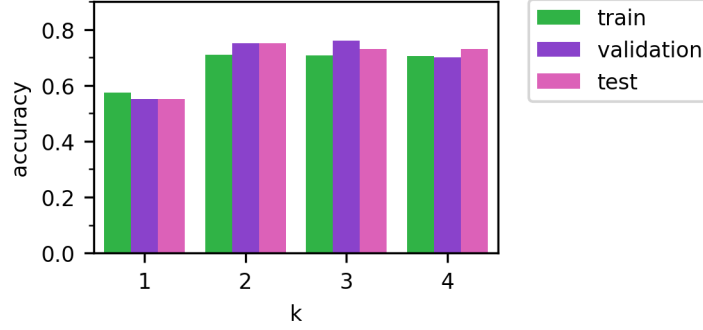


Figure 9: Training, validation, and testing accuracy vs K for SGC models.

sophisticated neural network architecture, increasing the dataset size, balancing the training set, conduct a more thorough grid search to optimize model hyperparameters during training, and so on. However, in addition to the model, there is another possible factor that limits the predictive performance of detecting AGG: the data itself. In the dataset used in this study a single candidate growth ratio is associated with each initial microstructure. However, the Monte Carlo Potts method is stochastic and the final results depend on the state of the random number generator during the simulation. Because of this it is possible for the same initial microstructure to exhibit either normal or AGG, depending on the random number generator. Therefore, the maximum meaningful accuracy that can be attained by a predictive model that only uses the initial state as an input is limited by the consistency of the simulations themselves.

To measure the dependency of candidate growth ratio on the random number generator, 3 trials each were picked from the training set that had reported candidate growth ratios close to 0, 5, 10, 15, and 20. The initial state was copied and the simulation was re-ran with a randomly selected seed. The growth ratio of the candidate grain was recorded and this process was repeated 20 times for each initial microstructure. The results are shown in Figure 10.

The violins are colored by the candidate growth ratios observed for the original data point from the training set used in this study, termed the 'original growth ratio.' From the plot it is clear that the final size of the candidate grain is heavily dependent on random state. Trials with original growth ratios of 0, indicating that the candidate grain was consumed in the original dataset, showed the lowest amount of variation. However, this set of trials still shows a wide range of growth ratio values both above and below 1. This indicates that even determining whether the candidate grows or shrinks is influenced by random state. In fact, one of the repeated trials contains candidate growth ratios that span from 0 to 9.75. Thus, despite having the same initial state the candidate grain was entirely consumed in one trial and grew so large that it almost met the criteria for abnormal growth in another.

Sets with an original growth ratio of 10 or 15 typically showed the highest amount of variation between repeated trials. Two out of three sets of trials with original candidate growth ratio values of 20 showed a lower median candidate growth ratio than two sets of trials with original candidate growth ratios of 15. In fact, both of these sets also had lower median values than one of the sets of trials with an original growth ratio of 10. This suggests that runs that exhibit growth ratios larger than about 15 are results of low-probability events instead of being a representative trial for that given initial microstructure.

The average value for the standard deviation of the candidate growth ratios for a given set of 20 repeated trials with the same initial structure, denoted σ , was found to be 3. Thus, a preliminary way to estimate the uncertainty in the dataset and selected criteria for AGG is to count the fraction of samples with growth ratios within 1σ of the threshold used for AGG. This corresponds to trials with candidate growth ratio values on the interval (7, 13). These samples have a high probability of flipping labels from AGG to normal grain growth, or vice versa, when re-run with a different random number seed.

About 35% of the samples in the training set meet this criteria. This indicates that an estimate of the upper bound for the maximum meaningful prediction accuracy is only 65%. This raises two issues. First, the maximum accuracy is only slightly better than random guessing for a given sample, indicating that there is an upper limit to the utility of developing classification models for this task. Second, the SGC model

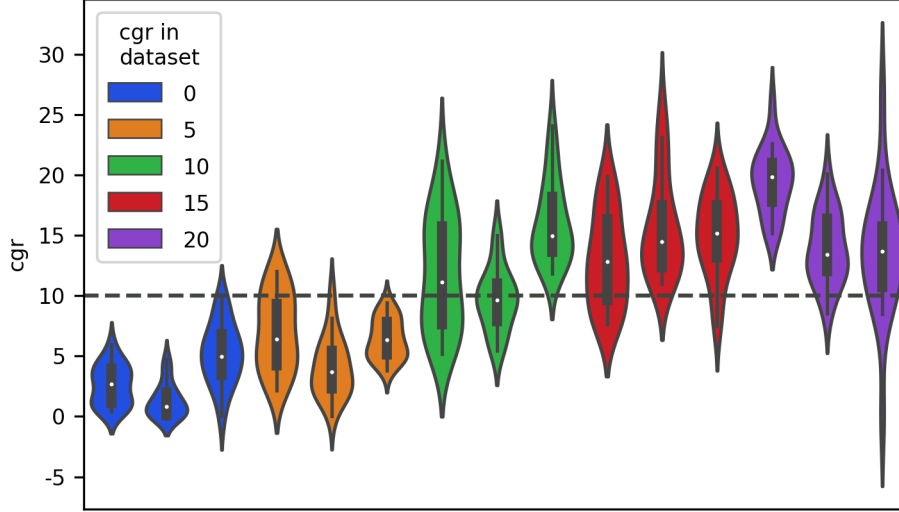


Figure 10: Candidate growth ratio (cgr) distributions for 20 simulations repeated for the same initial microstructure and different random number seeds for 15 different trials from the training set used in this study. Trials are colored by the corresponding cgr observed in the original dataset. Note that the distributions for each violin were determined from kernel density estimation and are thus purely statistical and not physical. This results in some distributions including negative values for cgr which are not physically possible.

achieved 75% accuracy on the validation and test sets, which is much higher than the estimated upper bound listed above. Since the test set was completely hidden from the model during training, performance of the model is representative of the predictive performance of the model in general.

The results indicate possible directions for future work. First, it is possible that using a more consistent definition of AGG will lead to less uncertainty. Uncertainty in the labels comes from both the intrinsic variation in the grain growth behavior observed in the simulation but also from the confidence in the ability of the criteria for AGG to separate the data into two distinct classes. Of course, the intrinsic uncertainty in the grain growth simulations due to the stochastic nature of the Monte Carlo simulations cannot be eliminated. For example, consider two trials conducted on the same initial state with different random seeds. In one trial, the candidate grain does not grow, and its final size is similar to initial size. In the second trial, the candidate grain undergoes several rapid bursts of growth and ends up significantly larger than the other grains in the matrix. In this case, the criteria for the label should not distinguish both of these runs as AGG or normal grain growth. Instead, the uncertainty associated with this initial state is accepted to be a consequence of the stochastic nature of the simulation.

However, there is also uncertainty associated with the criteria for determining the labels. This uncertainty can potentially be reduced by selecting more consistent labels. In this study, the criteria for AGG is when the candidate growth ratio exceeds 10. One limitation of this approach is that two trials with candidate growth ratios of 9.999 and 10.001 are labeled as normal and abnormal growth, despite having very similar growth trajectories in practice. This criteria would be reasonable if the distribution of growth ratios was bimodal and did not contain many trials with values close to the threshold. However, this is not the case for this dataset. The distribution of candidate growth ratio values is shown in Figure 11. The cumulative distribution increases approximately linearly between growth ratio values of 5 and 15, with an R^2 value of 0.997. Despite spanning a range of values from clear examples of normal growth to clear examples of AGG, the growth ratio values do not separate into two distinct regions. Thus, there will be several trials close to any threshold value selected in this range.

To reduce the uncertainty associated with the criteria for AGG, a more sophisticated process for distinguishing AGG from normal grain growth can be developed. From observing the trials it was determined that AGG occurs through sudden bursts of short-term growth. However, criteria like the growth ratio or the final relative sized used in ref [9] only use the initial and/or final grain sizes to characterize AGG. Thus,

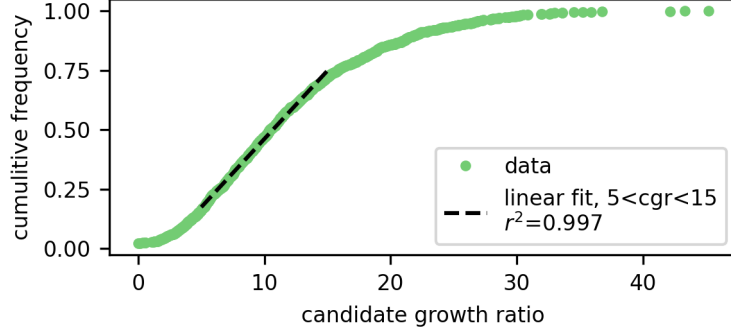


Figure 11: Cumulative distribution of candidate growth ratios in the training set used in this study.

these metrics only capture an average growth rate throughout the duration of the simulation. To obtain a more consistent criteria for detecting AGG, it is possible that analyzing the grain size at each time step to look for sudden growth events can provide a more objective criteria that better distinguishes between the two growth modes. This is one promising potential area of future work.

A second possible future direction for the project is to train models for regression or logistic regression instead of classification. Even with a better criteria to apply to distinguish between growth modes, the performance of any classification model is inherently limited by the stochastic nature of the Monte Carlo simulations. Thus, rather than assigning a single label to each initial state, predicting the overall distribution of candidate grain growth trajectories may be a more fruitful effort. The first step for this approach is to generate a new dataset containing grain growth simulations repeated several times for each initial state. Afterwards, there are several different approaches and possible project directions for exploring this further. One possibility would be to train a regression model to predict the mean and standard deviation values for the final size of the candidate grain in each set of repeated simulations for the same initial state. Another option would be to select a criteria for classifying AGG, and predict the fraction of repeated trials that will exhibit normal versus abnormal growth. Thus, instead of accepting the intrinsic variation of Monte Carlo simulations as a fundamental limitation that limits the utility of predictive models, this approach treats the variation itself as a signal that can be learned. This has the potential to provide additional insights about the growth mode of a material. In addition to predicting regions in a given microstructure that are likely to exhibit AGG, it may also be possible to detect regions which may have high amounts of variation in their microstructure evolution, prompting further investigation.

5 Conclusions

Two datasets of SPPARKS ‘candidate grain’ simulations of abnormal grain growth was created. Manual analysis of several simulations led to a preliminary working definition of abnormal grain growth. Two approaches for predicting the occurrence of abnormal grain growth using only the initial state of the system as an input. The first approach utilized a computer vision and transfer learning approach. The VGG16 convolutional neural network pre-trained on Imagenet was used to extract features from an image-based representation of the initial microstructure and a machine learning approach utilizing PCA and a kernel SVM classifier was used to predict which initial structures would exhibit abnormal grain growth. This approach only achieved 60% accuracy on the test set and showed signs of over-fitting to the training set. In the second approach, a simple graph convolution model was used to predict the occurrence of abnormal grain growth from a graph-based representation of the initial microstructure. This approach achieved 75% accuracy on the test set and did not show signs of over-fitting. Varying K, the number of iterations of message passing used by the model, indicated that only nearest and next-nearest neighbors of the candidate grain need to be considered to achieve the maximum performance observed in this study. The results did not support one hypothesis that a predictive model could achieve 80% accuracy, but did support a second hypothesis that the graph-based approach would outperform a similar computer vision model.

Investigation of the model performance lead to an investigation in the intrinsic uncertainty in grain growth behavior in the Monte Carlo simulations. Simulations were repeated using the same initial state and the only difference between repeated trials was the state of the random number generator. Significant variation was observed between repeated trials of each initial state. 35% of trials in the training set had a candidate growth ratio value that were close to the threshold used as a criteria for abnormal grain growth. This raises questions about the maximum possible meaningful predictive accuracy of abnormal grain growth attainable with the current dataset. Ongoing efforts to increase model performance include training models on a larger dataset and exploring more sophisticated model architectures and feature representations. Since significant variation was observed from the random state of the Monte Carlo simulations, additional efforts will be made to quantify the intrinsic uncertainty of these simulations and train models to predict the distribution of grain growth trajectories for each initial state, as opposed to a single target.

Acknowledgements

The authors acknowledge the Data-Driven Discovery of Optimized Multifunctional Material Systems (D3OM2S) Center of Excellence, Air Force agreement number FA8650-19-2-5209, for funding this project.

References

- [1] A. L. Etter, T. Baudin, and R. Penelle. Influence of the Goss grain environment during secondary recrystallisation of conventional grain oriented Fe-3%Si steels. *Scripta Materialia*, 47(11):725–730, December 2002. ISSN 13596462. doi: 10.1016/S1359-6462(02)00189-6.
- [2] Emilo Rinko, Iver Anderson, Aaron Kassen, Emma White, Wei Tang, Lin Zhou, Jason L Pries, and Matthew Kramer. Investigation of Powder Processing, Heat Treating, and Texturing to Improve Gas Atomized alnico Magnets for use in Electric Drive Motors. In *POWDER-MET 2019 Conference Proceedings*, page 61, 1390. URL <https://www.ornl.gov/publication/investigation-powder-processing-heat-treating-and-texturing-improve-gas-atomized-alnico>.
- [3] Timothy A. Furnish, Daniel C. Bufford, Fang Ren, Apurva Mehta, Khalid Hattar, and Brad L. Boyce. Evidence that abnormal grain growth precedes fatigue crack initiation in nanocrystalline Ni-Fe. *Scripta Materialia*, 143:15–19, January 2018. ISSN 13596462. doi: 10.1016/j.scriptamat.2017.08.047.
- [4] A. D. Rollett and W. W. Mullins. On the growth of abnormal grains. *Scripta Materialia*, 36(9):975–980, May 1997. ISSN 13596462. doi: 10.1016/S1359-6462(96)00501-5.
- [5] E. A. Holm, T. D. Hoffmann, A. D. Rollett, and C. G. Roberts. Particle-assisted abnormal grain growth. In *IOP Conference Series: Materials Science and Engineering*, volume 89. Institute of Physics Publishing, August 2015. doi: 10.1088/1757-899X/89/1/012005.
- [6] Rahbar Nasserrafi, Gerald E. Hicks, Michael A. Walker, and Craig M. Clasper. US20170175241A1 - Method to prevent abnormal grain growth for beta annealed ti-6al-4v forgings - Google Patents, 2017. URL <https://patents.google.com/patent/US20170175241A1/en>.
- [7] Kenta Yamanaka, Wataru Saito, Manami Mori, Hiroaki Matsumoto, Shigeo Sato, and Akihiko Chiba. Abnormal grain growth in commercially pure titanium during additive manufacturing with electron beam melting. *Materialia*, 6:100281, June 2019. ISSN 25891529. doi: 10.1016/j.mtla.2019.100281.
- [8] Ning Lu, Jiwoong Kang, Nancy Senabulya, Ron Keinan, Nicolas Gueninchault, and Ashwin J. Shahani. Dynamics of particle-assisted abnormal grain growth revealed through integrated three-dimensional microanalysis. *Acta Materialia*, May 2020. ISSN 13596454. doi: 10.1016/j.actamat.2020.04.049. URL <https://linkinghub.elsevier.com/retrieve/pii/S1359645420303177>.
- [9] Brian L. DeCost and Elizabeth A. Holm. Phenomenology of Abnormal Grain Growth in Systems with Nonuniform Grain Boundary Mobility. *Metallurgical and Materials Transactions A: Physical Metallurgy and Materials Science*, 48(6):2771–2780, June 2017. ISSN 10735623. doi: 10.1007/s11661-016-3673-6.

- [10] Justin Gilmer, Samuel S. Schoenholz, Patrick F. Riley, Oriol Vinyals, and George E. Dahl. Neural Message Passing for Quantum Chemistry. *34th International Conference on Machine Learning, ICML 2017*, 3:2053–2070, April 2017. URL <http://arxiv.org/abs/1704.01212>.
- [11] Miles D. Cranmer, Rui Xu, Peter Battaglia, and Shirley Ho. Learning Symbolic Physics with Graph Networks. *arXiv*, September 2019. URL <http://arxiv.org/abs/1909.05862>.
- [12] Kurt D Bollacker^{1f2}, Steve Lawrence², and C Lee Giles²¹³. CiteSeer: An Autonomous Web Agent for Automatic Retrieval and Identification of Interesting Publications. In *Proceedings of the second international conference on Autonomous agents - AGENTS '98*, pages 116–123, New York, New York, USA, 1998. ACM Press. ISBN 0897919831.
- [13] Cheol Woo Park, Mordechai Kornbluth, Jonathan Vandermause, Chris Wolverton, Boris Kozinsky, and Jonathan P. Mailoa. Accurate and scalable multi-element graph neural network force field and molecular dynamics with direct force architecture. *arXiv*, July 2020. URL <http://arxiv.org/abs/2007.14444>.
- [14] Alexey Strokach, David Becerra, Carles Corbi-Verge, Albert Perez-Riba, and Philip M. Kim. Fast and Flexible Protein Design Using Deep Graph Neural Networks. *Cell Systems*, 11(4):402–411.e4, October 2020. ISSN 24054720. doi: 10.1016/j.cels.2020.08.016.
- [15] SPPARKS Kinetic Monte Carlo Simulator, 2021. URL <https://spparks.github.io/index.html>.
- [16] Steve Plimpton, Corbett Battaile, Mike Chandross, Liz Holm, Aidan Thompson, Veena Tikare, Greg Wagner, Ed Webb, Xiaowang Zhou, Cristina Garcia Cardona, and Alex Slepoy. Crossing the Mesoscale No-Man’s Land via Parallel Kinetic Monte Carlo. Technical report, Sandia National Laboratories, 2009.
- [17] Karen Simonyan and Andrew Zisserman. Very Deep Convolutional Networks for Large-Scale Image Recognition. *arXiv*, September 2014. URL <http://arxiv.org/abs/1409.1556>.
- [18] Olga Russakovsky, Jia Deng, Hao Su, Jonathan Krause, Sanjeev Satheesh, Sean Ma, Zhiheng Huang, Andrej Karpathy, Aditya Khosla, Michael Bernstein, Alexander C. Berg, and Li Fei-Fei. ImageNet Large Scale Visual Recognition Challenge. *International Journal of Computer Vision*, 115(3):211–252, December 2015. ISSN 15731405. doi: 10.1007/s11263-015-0816-y.
- [19] Ian T. Jolliffe and Jorge Cadima. Principal component analysis: A review and recent developments, April 2016. ISSN 1364503X.
- [20] Corinna Cortes and Vladimir Vapnik. Support Vector Networks. *Machine Learning*, 20(3):273–297, 1995. ISSN 08856125. doi: 10.1007/BF00994018. URL <http://link.springer.com/10.1007/BF00994018>.
- [21] Kechen Song and Yunhui Yan. A noise robust method based on completed local binary patterns for hot-rolled steel strip surface defects. *Applied Surface Science*, 285:858–864, November 2013. ISSN 0169-4332. doi: 10.1016/J.APSUSC.2013.09.002. URL <https://www.sciencedirect.com/science/article/pii/S0169433213016437>.
- [22] Ryan Cohn and Elizabeth Holm. Unsupervised Machine Learning Via Transfer Learning and k-Means Clustering to Classify Materials Image Data. *Integrating Materials and Manufacturing Innovation*, 10(2):231–244, 2021. ISSN 2193-9772. doi: 10.1007/s40192-021-00205-8. URL <https://doi.org/10.1007/s40192-021-00205-8>.
- [23] Stéfan van der Walt, Johannes L. Schönberger, Juan Nunez-Iglesias, François Boulogne, Joshua D. Warner, Neil Yager, Emmanuelle Gouillart, and Tony Yu. scikit-image: image processing in Python. *PeerJ*, 2:e453, June 2014. ISSN 2167-8359. doi: 10.7717/peerj.453. URL <https://peerj.com/articles/453>.
- [24] Felix Wu, Tianyi Zhang, Amauri Holanda de Souza, Christopher Fifty, Tao Yu, and Kilian Q. Weinberger. Simplifying Graph Convolutional Networks. *36th International Conference on Machine Learning, ICML 2019*, 2019-June:11884–11894, February 2019. URL <http://arxiv.org/abs/1902.07153>.

- [25] Prithviraj Sen, Galileo Namata, Mustafa Bilgic, Lise Getoor, Brian Galligher, and Tina Eliassi-Rad. Collective classification in network data. *AI magazine*, 29(3):93, 2008.
- [26] Diederik P. Kingma and Jimmy Lei Ba. Adam: A method for stochastic optimization. In *3rd International Conference on Learning Representations, ICLR 2015 - Conference Track Proceedings*. International Conference on Learning Representations, ICLR, December 2015. URL <https://arxiv.org/abs/1412.6980v9>.